Nonsymmetric Interactions Trigger Collective Swings in Globally Ordered Systems

Andrea Cavagna,[1,2] Irene Giardina,[1,2,3] Asja Jelic,[1,2,4] Stefania Melillo,[1,2] Leonardo Parisi,[1,2,5] Edmondo Silvestri,[1,6] and Massimiliano Viale[1,2]

[1]*Istituto Sistemi Complessi, Consiglio Nazionale delle Ricerche, UOS Sapienza, 00185 Rome, Italy*
[2]*Dipartimento di Fisica, Università Sapienza, 00185 Rome, Italy*
[3]*INFN, Unità di Roma 1, 00185 Rome, Italy*
[4]*The Abdus Salam International Centre for Theoretical Physics, Strada Costiera 11, 34014 Trieste, Italy*
[5]*Dipartimento di Informatica, Università Sapienza, 00185 Rome, Italy*
[6]*Dipartimento di Fisica, Università di Roma 3, 00146 Rome, Italy*

(Received 10 May 2016; revised manuscript received 28 December 2016; published 31 March 2017)

Many systems in nature, from ferromagnets to flocks of birds, exhibit ordering phenomena on the large scale. In condensed matter systems, order is statistically robust for large enough dimensions, with relative fluctuations due to noise vanishing with system size. Several biological systems, however, are less stable and spontaneously change their global state on relatively short time scales. Here we show that there are two crucial ingredients in these systems that enhance the effect of noise, leading to collective changes of state on finite time scales and off-equilibrium behavior: the nonsymmetric nature of interactions between individuals, and the presence of local heterogeneities in the topology of the network. Our results might explain what is observed in several living systems and are consistent with recent experimental data on bird flocks and other animal groups.

DOI: 10.1103/PhysRevLett.118.138003

Ordering phenomena are ubiquitous in nature, spanning from ferromagnetism and structural transitions in condensed matter, to collective motion in biological systems, and consensus dynamics in social networks. Order by itself requires a notion of robustness: the degree of global coordination must be stable in spite of noise, at least on certain time scales. This concept is quantified rigorously in equilibrium statistical physics: a system exhibits long range order when the relative fluctuations of the global order parameter are vanishingly small in the thermodynamic limit. In a finite system, due to noise, global order can fluctuate, but fluctuations are so small that bringing the system away from its original state would take a huge amount of time; the larger the size of the system, the longer the time.

Many ordered biological systems, however, exhibit a larger sensitivity to noise and can change their state on relatively short time scales. Flocks of birds, for example, have very large polarization but they spontaneously turn and change their flight direction very frequently [1,2]. Consensus in social networks can swiftly switch from a selected choice to another [3]. Fluctuations appear to have a dominant role and one might wonder what kind of mechanism is responsible for this behavior, and whether it implies a disruption of long range order in the statistical physics sense.

In this Letter we show that there are two crucial ingredients in these systems that enhance the effect of noise leading to collective changes of state: the nonsymmetric nature of interactions between individuals, and the presence of local heterogeneities in the topology of the interaction network. Surprisingly, the consequences of these two features can be larger the larger the system size leading to a relaxation time that remains finite at large sizes. The system keeps changing its global state in time, being constantly driven out of equilibrium by spontaneous fluctuations. Besides, we show that big fluctuations typically build up at the boundary, peripheral nodes acting as triggers for the global change. Our analysis might explain what is observed in several living systems and is consistent with recent experimental results on wild flocks [1] and laboratory fish schools [4].

The archetypical case of global order in statistical physics is the ferromagnet, described by the classical Heisenberg model on a d-dimensional lattice. The Hamiltonian of the system is $\mathcal{H} = -J/2\sum_{ij} n_{ij}\vec{\sigma}_i \cdot \vec{\sigma}_j$ where $\vec{\sigma}_i \in \mathbb{R}^d$ are norm one vectors, and the adjacency matrix $n_{ij} = n_{ji}$ is equal to 1 for neighboring sites in the lattice, and 0 otherwise. For $d > 2$, the Heisenberg model has an ordering transition at finite temperature T_c. For $T < T_c$, the system exhibits a spontaneous magnetization $\vec{M} = (1/N)\sum_i \vec{\sigma}_i = M\vec{n}$, all spins pointing on average in the same direction $\vec{n}$. For a system of size N, the time needed for the system to change the direction of the magnetization—the relaxation time τ_N—grows with the system size, ensuring stability of order in the thermodynamic limit [5–7]. The Heisenberg model offers the simplest example of imitative interaction rules that are commonly used to model biological and social groups [8–11]. For these systems, however, interactions are often nonreciprocal and individuals do not sit on a lattice. We will therefore consider a generalization of the Heisenberg model where n_{ij} can be nonsymmetric and has an irregular spatial

structure, and explore how these features affect the relaxation behavior of the system.

The mechanism of relaxation at low temperature can be well illustrated by a simple computation. Each spin can be rewritten in terms of a longitudinal and a perpendicular component, $\vec{\sigma}_i = \sigma_i^L \vec{n} + \vec{\pi}_i$. At low T, $M \sim 1$, $|\vec{\pi}_i|^2 \ll 1$, and $\sigma_i^L \sim 1 - |\vec{\pi}_i|^2/2$. The system is then fully described by the perpendicular fluctuations. To compute the relaxation time, we need to specify what is the dynamics followed by the system. We consider a Langevin dynamics with both dissipative and inertial terms, covering a variety of dynamical behaviors in condensed matter [6,7,12,13] and biological groups [1,2,9,14,15]. The alignment force acting on each spin i is $\vec{\mathcal{F}}_i^{\rm al} = J\sum_j n_{ij}\vec{\sigma}_j$. The only part of this force preserving the norm of $\vec{\sigma}_i$ (and therefore entering the dynamical equations) is $\vec{\mathcal{F}}_i = [\vec{\mathcal{F}}_i^{\rm al}]^{\perp} = \vec{\mathcal{F}}_i^{\rm al} - (\vec{\mathcal{F}}_i^{\rm al}\cdot\vec{\sigma}_i)\vec{\sigma}_i$. Expanding at low T we get $\vec{\mathcal{F}}_i \sim -J\sum_j \Lambda_{ij}\vec{\pi}_j$, where $\Lambda_{ij} = -n_{ij} + \delta_{ij}\sum_k n_{ik}$ is the discrete Laplacian. The dynamical equations for the $\{\vec{\pi}_i\}$ then read [16]

$$\chi\frac{d^2\vec{\pi}_i}{dt^2} = -J\sum_j \Lambda_{ij}\vec{\pi}_j - \eta\frac{d\vec{\pi}_i}{dt} + \vec{\xi}_i, \tag{1}$$

where χ and η represent, respectively, a rotational inertia and a rotational viscosity; and $\vec{\xi}_i$ is a Gaussian noise with $\langle\vec{\xi}_i(t)\cdot\vec{\xi}_j(t')\rangle = 2T(d-1)\eta\delta_{ij}\delta(t-t')$. By taking the limit $\chi/\eta^2 \to 0$ we recover a purely overdamped dynamics [6,7,14,17–20], while $\eta \to 0$ corresponds in the symmetric case to a reversible Hamiltonian dynamics [1,2,13].

Let us assume that at time $t = 0$ the system is in a polarized state with $\vec{M} = \vec{M}_0$. The magnetization then fluctuates in time due to the spontaneous noise. From Eq. (1) one can compute the perpendicular fluctuation $\delta\vec{M}^{\perp} = (1/N)\sum_i\vec{\pi}_i$ of the magnetization with respect to $\vec{M}_0$, measuring how much the system has departed from the original direction. One finds (see Supplemental Material [21])

$$\langle|\delta\vec{M}^{\perp}|^2\rangle = D\frac{t}{\eta} + F_{\rm dyn}(t),$$
$$D = \frac{2(d-1)T}{N}\sum_i (u_i^0)^2, \tag{2}$$

where $\langle\cdots\rangle$ are averages over the noise, and we introduced the diffusion coefficient D. Here $\mathbf{u^0}$ is the N-dimensional left lowest eigenvector of the Laplacian, and corresponds to a zero (Goldstone) mode resulting from the rotational symmetry of the interactions. $F_{\rm dyn}(t)$ is a subdominant (in time) contribution. When $|\delta\vec{M}^{\perp}| \sim O(1)$, the system has changed its global direction. Since the term in D dominates in Eq. (2), this occurs when $t/\eta \sim 1/D$, giving the relaxation time

$$\frac{\tau}{\eta} \sim \frac{1}{D}. \tag{3}$$

Equations (2) and (3) connect the relaxation of the system (a dynamical quantity) with the spectral properties of the Laplacian (a topological feature of the network).

For the standard Heisenberg model on a regular lattice, Eq. (3) further simplifies. In this case n_{ij} and Λ_{ij} are symmetric and left and right eigenvectors coincide. Given that $\sum_j\Lambda_{ij} = 0$, $\mathbf{u^0}$ is a real constant vector. For a system of size N one has $u_i^0 = 1/\sqrt{N}$, giving a diffusion coefficient $D \sim 1/N$ and the well-known scaling for the relaxation time $\tau_N \sim N$ [6,7]. The interpretation of this result is illuminating. When the system orders, it spontaneously chooses a direction among all the possible ones. There remain, however, "easy fluctuations" in the manifold perpendicular to $\vec{M}$ that is described by the zero eigenspace of the Laplacian. In the presence of noise, the system moves along these soft modes: fluctuations are small but build up in time leading to the diffusive behavior of the magnetization. Because of the homogeneity of the interaction network, fluctuation modes are delocalized: each spin equally contributes with a vanishing weight leading to the divergence of the relaxation time with size, and to stability of order in the thermodynamic limit. There are also nontrivial space-time correlations [5,12] describing how fluctuations are transmitted through the system, and getting contributions from all modes. The average effect of fluctuations on the magnetization is captured by the zero mode only, see Eq. (2).

Let us now consider an n_{ij} matrix better characterizing real biological networks. As already mentioned, interactions are not necessarily symmetric. Animals in a group, for example, usually perceive neighbors who are not themselves able to see them. Besides, the lattice structure is restrictive since many biological systems do not exhibit structural order in space [8,28]. The simplest thing we can do is to draw points uniformly in Euclidean space instead of using a regular lattice. Then we place the spins on such points and prescribe that each spin interacts with its first n_c neighbors. Since neighbors are not reciprocal off lattice, what we get is an alignment model on a random Euclidean network with a nonsymmetric n_{ij} (where $n_{ij} = 1$ if j is one of the first n_c nearest neighbors of i, and 0 otherwise). We call this model the nonsymmetric Euclidean random Heisenberg (NERH) model. For $d = 3$ and $n_c = 6$ this system has the same dimensionality and connectivity as the standard Heisenberg model, but with $n_{ij} \neq n_{ji}$. Natural flocks of birds exhibit a similar typology of interaction network [10,11,29–31] and obey a dynamics of the kind of Eq. (1) in the underdamped limit [1,15,32]. More generally, there may be other factors contributing to the asymmetry, like anisotropies in the interactions or individual heterogeneities. Here we consider the asymmetry due to mere structural properties.

When interactions are nonsymmetric, detailed balance is not obeyed and we can expect off-equilibrium features [16,33]. Besides, n_{ij} is now a random matrix belonging to the class of non-Hermitian Euclidean random matrices [34,35], with nontrivial spectral properties. The NERH model might therefore lead to novel dynamical behavior.

Let us now use Eqs. (2) and (3) to investigate the relaxation properties of the model. Contrary to the symmetric case, both n_{ij} and Λ_{ij} have right and left eigenvectors that behave differently. In particular, $\mathbf{u^0}$ is not a constant vector and depends on the specific network considered. Different networks have different $\mathbf{u^0}$, different D, and, consequently, different relaxation properties. To explore Eqs. (2) and (3) we have therefore generated many samples of NERH networks of size N. Each network was obtained by drawing at random N points in a $3d$ sphere, and building the asymmetric spin-spin interaction graph as discussed above. For each network, we computed numerically $\mathbf{u^0}$ (see Supplemental Material [21]), and evaluated the diffusion coefficient as defined in Eq. (2). Then, given a network, we performed a numerical simulation of its dynamical evolution (Eq. (1) and Supplemental Material [21]). We considered the system in the low temperature region ($M \sim 0.98$) and evaluated the relaxation time τ as the time where $\langle|\delta\vec{M}^{\perp}(t)|^2\rangle \sim O(1)$ [see Fig. 1(a)]. In Fig. 1(b) we plot the relaxation time (computed from the dynamics) as a function of the diffusion coefficient (computed from the network) for networks with $N = 1000$. This figure shows that the relaxation time indeed scales inversely with the diffusion coefficient, independently of the dissipative or reversible character of the dynamics, as predicted by Eqs. (2) and (3) (with larger error bars in the overdamped case, see Supplemental Material [21]).

The relaxation time of the system thus crucially depends on the properties of $\mathbf{u^0}$, the left eigenvector. In particular, u_i^0—also known as the *eigenvalue centrality* of node i [36]—can vary from node to node determining different contributions to the global fluctuations. If $\mathbf{u^0}$ is extended (similarly to what happens in a regular lattice) then centrality is homogeneously distributed through the network, $D \sim 1/N$ and the relaxation time is proportional to the size N of the system. If, however, $\mathbf{u^0}$ is localized on a finite subset of nodes, the diffusion coefficient could be substantially larger leading to much shorter relaxation times. The distribution of D in the network ensemble for $N = 1000$, $n_c = 6$ is plotted in Fig. 1(c). This distribution has a large main peak centered on the value $D \sim 1/N$ indicating that most of the networks behave in a homogeneous manner and have a small diffusion coefficient, as in the Heisenberg model on a regular lattice. There are, however, a few networks with a substantially larger diffusion coefficient, corresponding to the secondary peak of the distribution. The homogenous networks with small D have long relaxation times, while the few ones with large D relax on much quicker scales.

We therefore find a bimodality in the distribution of the diffusion coefficient and, consequently, of the relaxation time. To understand the relevance of this result we need to understand how the distribution $P(D)$ changes with the system size. To this aim, we have generated ensembles of NERH networks for different values of N ranging from $N = 128$ to $N = 65536$. For each ensemble of size N, we computed the distribution $P(D)$. The resulting curves are plotted in Fig. 2(a). What we see is that (i) the primary peak is centered on a value of D that decreases with system size (see inset) as would happen for symmetric networks, and (ii) the secondary peak is instead always peaked on the same finite value $D \sim (d-1)T/n_c$ and its height *increases* with the size N of the network. We also computed the global probability of finding a network with finite D, defined as the integral over the secondary peak. As can be seen from Fig. 2(b), this probability increases with N: the occurrence

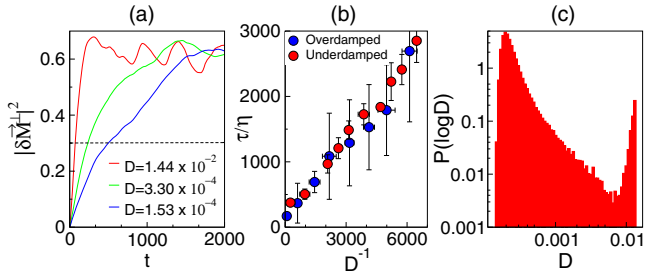

FIG. 1. (a) Perpendicular fluctuation of the magnetization as a function of time, for three networks with different diffusion coefficients (underdamped dynamics). The relaxation time is the time where $\langle|\delta\vec{M}^{\perp}(t)|^2\rangle = 0.3$ (black dotted line). (b) Relaxation time vs diffusion coefficient; networks are binned in $1/D$, and τ is then averaged inside each bin (error bars are standard deviations). (c) Probability distribution of the diffusion coefficient; we plot the distribution of $\log(D)$ to better visualize the secondary peak. NERH ensemble with $N = 1000$ and $n_c = 6$. The parameters of the dynamics are: $J = 1.2$, $T = 0.024$, $\chi = 0.83$, $\eta = 15$, 30, 60 (overdamped dynamics), $\eta = 0.3$ (underdamped dynamics).

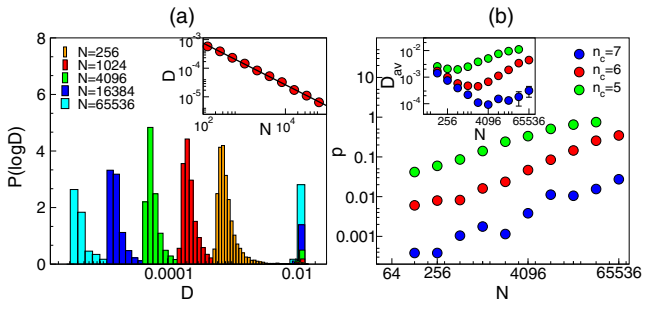

FIG. 2. (a) Probability distribution of the diffusion coefficient for NERH ensembles of different size. $N \in [128:65536]$; $n_c = 6$. Inset: Value of D at the primary peak, as a function of the network size; the black line has slope -1. (b) Probability of the secondary peak as a function of the network size, for NERH ensembles with different n_c. Inset: Average diffusion coefficient as a function of network size.

of networks with a finite diffusion coefficient is not, therefore, a finite size effect. On the contrary, these networks are statistically more relevant the larger the system size. Indeed the average over the ensemble of the diffusion coefficient starts increasing at large enough N [Fig. 2(b), inset]. These results hold for different values of n_c, with a faster increase for smaller n_c [see Fig. 2(b)]. Nonsymmetric interactions can therefore have a dramatic impact on the relaxation of the system: if we draw at random a NERH network, it will have, with finite probability, a finite relaxation time, no matter how large the network is.

Let us now discuss the localization properties of the eigenvector $\mathbf{u^0}$. We can compute the participation ratio $\mathrm{PR} = (\sum_i (u_i^0)^2)^2 / \sum_i (u_i^0)^4$, a quantity that scales as the number of sites where the mode is localized [37]. While for slow networks PR increases with N (extended mode), for the quick networks with a finite diffusion coefficient $\mathrm{PR} \sim n_c$ [see Fig. 3(a)]. This means that in the quick networks there are approximately n_c nodes that dominate the collective fluctuations. Besides, these most influent nodes are closely located in space and very connected one to the other, as quantified by the high value of the clustering coefficient $c_i = 1/[n_c(n_c-1)] \sum_{jk} n_{ij} n_{ik} n_{jk}$ [for $N = 1000$ $\langle c_i \rangle = 0.90 \pm 0.11$—see also Fig. 3(b)]. This highly clustered region also tends to be poorly connected with the rest of the network (due to the finite connectivity), and it is responsible for the nonstandard response of the system to noise. To see this, let us consider the extreme situation where the network consists exactly of a small cluster of n_c nodes *all* connected with one another ($c_i = 1$), and a large homogeneous cluster of $N - n_c$ nodes with a few links pointing to the small one. The small cluster evolves independently of the large one and therefore exhibits global fluctuations of order [according to Eq. (2)] $\langle |\delta \vec{M}^{\perp}|^2 \rangle \sim t/n_c$. Thus, it will change its state on short scales $\tau \sim n_c$. The large cluster would by itself fluctuate much less, but due to the connections to the small cluster it is dragged from its original direction and the relaxation time of the whole network is drastically decreased.

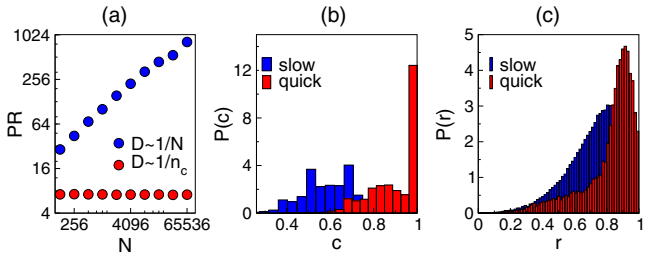

FIG. 3. (a) Participation ratio as a function of network size, for quick networks (red points) and slow networks (blue points). $N \in [128:65536]$; $n_c = 6$. (b) Distribution probability of the clustering coefficient of the n_c most influent nodes (see text) for quick (red) and slow (blue) networks. $N = 1000$; $n_c = 6$. (c) Distribution probability of the normalized distance from the network's center for the same nodes as in panel (b).

The occurrence of almost disconnected clusters has statistical origins. When we draw nodes at random in space and build the interaction graph, we can by mere chance produce a clump of n_c close nodes. The probability of such a local heterogeneity can be very small (depending on the value of n_c), but it only depends on the local properties of the network. Thus, as in typical nucleation processes, the larger the system the larger is the chance that somewhere in the network one of such regions occurs, explaining the growth of the secondary peak with size. Close to the boundary, nodes have neighbors only in half of the available space, potentially increasing local clustering. Indeed Fig. 3(c) shows that the regions with large u_i^0 and c_i tend to be located at the periphery of the network, with typical normalized distance r from the network center of order $r \sim 0.9$ ($r = 0$ corresponding to the center, $r = 1$ to the border). Thus, even though asymmetry is the primary condition to obtain a finite relaxation time, the network must also be sufficiently heterogeneous to allow for localized eigenvectors. NERH networks—due to their embedding in space—allow for local clustering and localization (contrary to other kinds of random Laplacian graphs [38]).

So far we analyzed the NERH ensemble. Our results, however, rely on a few very general properties: a direct interaction graph with finite connectivity (local asymmetric interactions) and an imitative dynamics (mutual alignment). Besides, they qualitatively hold when changing the details of the interaction. For example, similar results are obtained when introducing a hard core between individuals or assuming that individuals at the border interact with a different number of neighbors (see Fig. S2 and Supplemental Material [21]). For this reason, our analysis provides an attractive route to explain how spontaneous collective swings occur in real instances of coordinated behavior. In many biological cases, the interaction network is not fixed but evolves dynamically. Flocks of birds, for example, at a given instant of time have an interaction graph that shares some of the NERH features (individuals homogeneously distributed in space, an average given number of interacting neighbors [10,29]). As birds exchange positions in space the graph will progressively change. A single flock explores during its motion many different realizations of asymmetric random graphs, the dynamics playing the role of the ensemble for the NERH model. Therefore, in the absence of predation, we expect the flock to spontaneously change direction of motion whenever a "quick" graph with a large diffusion coefficient is visited. Asymmetric interactions can also modify the hydrodynamic behavior of very large flocks, as discussed in Ref. [39] for longitudinal asymmetries. Even though the focus of our Letter is different, both works point out that nonsymmetric interactions can have a fundamental role—distinct from motility—in the nonequilibrium behavior of active systems.

Testing our predictions directly on real data is not straightforward, because we do not know *a priori* the interaction graph

between individuals. In natural flocks, inference techniques allowed us to extract the average connectivity n_c [10,29–31], but retrieving the entire graph requires experimental statistics not available to date. There are, however, several experimental observations that are consistent with our findings and support our explanation. Flocks of birds indeed exhibit spontaneous coherent turns very frequently even for large group sizes [1]. Besides, all turns start from the lateral periphery of the flock and initiators are individuals displaying unusual directional fluctuations [2]. A new analysis on flocks data also shows that the network topology is heterogeneous prior to turns [40]. These facts—not explained by symmetric flocking models [14]—are instead predicted by the NERH modeling. Recent results on fish schools [4] show that these groups occasionally display spontaneous evasion waves. Also in this case, initiators of the startle events are located peripherally and have a large clustering coefficient, in line with our results.

For a biological group, controlling and regulating collective behavior has a crucial role. The group must maintain a large sensitivity to perturbations to ensure efficient collective responses (as in antipredatory maneuvers), and at the same time retain group coherence. The mechanism we described shows how to achieve such a marginal stability: the system is always highly ordered but off-equilibrium effects allow for rapid collective swings.

We thank V. Martin Major, T. Mora, S. Ramaswamy, and A. Walczak for discussions, and S. Ramaswamy for sharing his preliminary draft of Ref. [39]. This work was supported by grants IIT–Seed Artswarm, ERC–StG No. 257126 and US-AFOSR—FA95501010250 (through the University of Maryland).

[1] A. Attanasi, A. Cavagna, L. D. Castello, I. Giardina, T. S. Grigera, A. Jelic, S. Melillo, L. Parisi, O. Pohl, E. Shen, and M. Viale, Nat. Phys. **10**, 691 (2014).
[2] A. Attanasi, A. Cavagna, L. D. Castello, I. Giardina, A. Jelic, S. Melillo, L. Parisi, O. Pohl, E. Shen, and M. Viale, J. R. Soc. Interface **12**, 20150319 (2015).
[3] D. Centola, Science **329**, 1194 (2010).
[4] S. B. Rosenthal, C. R. Twomey, A. T. Hartnett, H. S. Wu, and I. D. Couzin, Proc. Natl. Acad. Sci. U.S.A. **112**, 4690 (2015).
[5] G. Parisi, *Statistical Field Theory.* (Addison-Wesley, Redwood City, 1988).
[6] Y. Y. Goldschmidt, Nucl. Phys. **B280**, 340 (1987).
[7] J. C. Niel and J. Zinn-Justin, Nucl. Phys. **B280**, 355 (1987).
[8] I. D. Couzin and J. Krause, Adv. Study Behav. **32**, 1 (2003).
[9] T. Vicsek and A. Zafeiris, Phys. Rep. **517**, 71 (2012).
[10] W. Bialek, A. Cavagna, I. Giardina, T. Mora, E. Silvestri, M. Viale, and A. M. Walczak, Proc. Natl. Acad. Sci. U.S.A. **109**, 4786 (2012).
[11] W. Bialek, A. Cavagna, I. Giardina, T. Mora, O. Pohl, E. Silvestri, M. Viale, and A. M. Walczak, Proc. Natl. Acad. Sci. U.S.A. **111**, 7212 (2014).
[12] P. C. Hohenberg and B. I. Halperin, Rev. Mod. Phys. **49**, 435 (1977).
[13] P. M. Chaikin and T. C. Lubensky, *Principles of Condensed Matter Physics* (Cambridge University Press, Cambridge, England, 2000), Vol. 1.
[14] T. Vicsek, A. Czirok, E. Ben-Jacob, I. Cohen, and O Shochet, Phys. Rev. Lett. **75**, 1226 (1995).
[15] A. Cavagna *et al.*, J. Stat. Phys. **158**, 601 (2015).
[16] R. Zwanzig, *Nonequilibrium Statistical Mechanics* (Oxford University Press, Oxford, 2001).
[17] Y. Tu, J. Toner, and M. Ulm, Phys. Rev. Lett. **80**, 4819 (1998).
[18] I. D. Couzin, J. Krause, R. James, G. D. Ruxton, and N. R. Franks, J. Theor. Biol. **218**, 1 (2002).
[19] G. Grégoire and H. Chaté, Phys. Rev. Lett. **92**, 025702 (2004).
[20] F. Ginelli and H. Chaté, Phys. Rev. Lett. **105**, 168103 (2010).
[21] See Supplemental Material at http://link.aps.org/supplemental/10.1103/PhysRevLett.118.138003, which includes Refs. [22–27], for details on the computation leading to Eq. (2) and on the procedure used to analyze the NERH networks, a description of the numerical simulations, and results on NERH models with hard core and boundary effects.
[22] C. M. Bender and S. A Orszag, *Advanced Mathematical Methods for Scientists and Engineers I* (Springer Science & Business Media, New York, 1999).
[23] D. Cassi, Phys. Rev. Lett. **68**, 3631 (1992).
[24] M. Castellana, W. Bialek, A. Cavagna, and I. Giardina, Phys. Rev. E **93**, 052416 (2016).
[25] M. Ballerini *et al.*, Animal Behaviour **76**, 201 (2008).
[26] A. Strandburg-Peshkin *et al.*, Curr. Biol. **23**, R709 (2013).
[27] R. G. Martin, J. Comp. Physiol. A **159**, 545 (1986).
[28] A. Cavagna, A. Cimarelli, I. Giardina, A. Orlandi, G. Parisi, A. Procaccini, R. Santagati, and F. Stefanini, Math. Biosci. **214**, 32 (2008).
[29] M. Ballerini *et al.*, Proc. Natl. Acad. Sci. U.S.A. **105**, 1232 (2008).
[30] A. Cavagna, L. D. Castello, S. Dey, I. Giardina, S. Melillo, L. Parisi, and M. Viale, Phys. Rev. E **92**, 012705 (2015).
[31] T. Mora, A. M. Walczak, L. D. Castello, F. Ginelli, S. Melillo, L. Parisi, M. Viale, A.Cavagna, and I. Giardina, Nat. Phys. **12**, 1153 (2016).
[32] A. Cavagna, I. Giardina, T. S. Grigera, A. Jelic, D. Levine, S. Ramaswamy, and M. Viale, Phys. Rev. Lett. **114**, 218101 (2015).
[33] G. Young, L. Scardovi, and N. Leonard, *Proceedings of American Control Conference (ACC)* (IEEE, New York, 2010), p. 6312.
[34] M. Mézard, G. Parisi, and A. Zee, Nucl. Phys. **B559**, 689 (1999).
[35] A. Goetschy and S. E. Skipetrov, Phys. Rev. E **84**, 011150 (2011).
[36] P. Bonacich and P. Lloyd, Soc. Networks **23**, 191 (2001).
[37] J. T. Edwards and D. J. Thouless, J. Phys. C **5**, 807 (1972).
[38] N. Perra, V. Zlatić, A. Chessa, C. Conti, D. Donato, and G. Caldarelli, Europhys. Lett. **88**, 48002 (2009).
[39] L. P. Dadhichi, R. Chaijwa, A. Maitra, and S. Ramaswamy, arXiv:1605.00981.
[40] We computed the distribution of the $\{u_i^0\}$ using the approximate graph built with the inferred average n_c.